JCTC Journal of Chemical Theory and Computation

ARTICLE

pubs.acs.org/JCTC

Toward Reliable DFT Investigations of Mn-Porphyrins through CASPT2/DFT Comparison

Mikael Kepenekian,[†,‡] Adrian Calborean,[†] Valentina Vetere,[†,∥] Boris Le Guennic,[‡] Vincent Robert,[*,‡,§] and Pascale Maldivi[*,†]

[†]SCIB, UMR_E 3 CEA/UJF-Grenoble 1, Laboratoire de Reconnaissance Ionique et Chimie de Coordination, INAC, Grenoble, F-38054, France

[‡]Université de Lyon, CNRS, Institut de Chimie de Lyon, Ecole Normale Supérieure de Lyon, 15 Parvis René Descartes, 69342 Lyon Cedex 07, France

[§]Laboratoire de Chimie Quantique, Institut de Chimie de Strasbourg, UMR7177 CNRS/Université de Strasbourg, 4, rue Blaise Pascal, CS 90032, 67081 Strasbourg-Cedex, France

ABSTRACT: The low-energy spectroscopies of Mn(II) and Mn(III) porphyrin (P) complexes were investigated using complete active space and subsequent perturbative treatment (CASPT2) as well as DFT-based calculations. Starting from DFT optimizations of $Mn^{II}P$ and $Mn^{III}PCl$ using crystallographic data, the CASPT2 results show that whatever the relative position of the Mn(II) ion with respect to the porphyrin cavity, the high-spin state $S = 5/2$ of the [MnP] unit lies much lower in energy than the intermediate $S = 3/2$ state. Not only are these results in agreement with experimental observations but they also differ from previous theoretical conclusions. In the Mn(III) complexes, σ and π charge redistributions compete to result in a $S = 2$ ground state. The performances of different functionals have been tested in the reproduction of the CASPT2 spin gaps. Our results confirm that the Mn(II) system is very challenging, as GGA functionals fail in the spin states ordering and in the reproduction of the gaps, unless a high percentage of exact HF exchange (55%), as in KMLYP, is incorporated. This inspection demonstrates the need for specific active space functional to investigate the low-energy spectroscopy of [MnP] units.

1. INTRODUCTION

The prominent role of porphyrin-based complexes in biological processes as in heme active sites has stimulated intense work from both the experimental and theoretical communities since the 1970s.[1−5] Much attention has been devoted to revealing the strong relationships between the electronic structures of metalloporphyrins and their molecular parameters. Such remarkable interplay has also led to intense efforts in order to take advantage of these features in widespread areas of interest such as health, catalysis,[6−8] and molecular materials.[9] In particular, metalloporphyrins have been recently investigated as possible information storage devices taking advantage of charge transfer effects.[10−13] The association of a redox metal center such as manganese with smart functionalization of the porphyrin has turned out to be a promising route in the design of molecular switches.[14] From this perspective, we got interested in gaining a better understanding of the particular relationships between the electronic structures of Mn(II) and Mn(III) porphyrins and their structural features through theoretical approaches.

Quantum chemistry descriptions of metalloporphyrins are well documented in the literature, especially after the advent of density functional theory (DFT) methods.[15−23] This class of coordination compounds is also considered a good candidate for quantum chemistry benchmarking,[19−23] thanks to the large amount of chemical and spectroscopic data available. The most difficult case is for Mn(II) (d^5), which may give rise to two low-lying states: the high-spin one (HS, $S = 5/2$) and an intermediate one (IS, $S = 3/2$). Much experimental evidence (Mn−N distances, EPR, magnetic data) has unambiguously shown that the sextet is the ground state.[24−26] In contrast, from the early extended Hückel calculations[3] to more recent DFT studies,[20,27] the electronic structure of Mn(II) porphyrins is predicted to exhibit a quartet ground state. In particular, it seems that GGA functionals are unable to reproduce the high-spin character of the ground state. In contrast, hybrid functionals which contain a Hartree−Fock exchange component do predict most of the time the correct spin energetics.[20] This result is in line with the well-known property of hybrid functionals to favor the HS state as ground state, contrarily to GGA predicting generally a low spin state.[28−30] It was long ago underlined[1,26] that the HS state of Mn(II) implies the population of a $d_{x^2-y^2}$ orbital compared to its IS state (or to Mn(III), d^4) thus leading to significantly longer Mn−N distances in HS Mn(II) porphyrins (d_{Mn-N} *ca.* 2.09 Å) compared to IS six-coordinate ones (d_{Mn-N} *ca.* 2.03 Å) or to HS ($S = 2$) Mn(III) porphyrins (d_{Mn-N} *ca.* 2.02 Å).[26] Actually, X-ray structural studies have clearly shown that the Mn(II) ion is positioned out of the mean porphyrinic plane at a height of 0.19 Å in a tetra-coordinated Mn(II) tetraphenyl porphyrin (TPP).[24,26] Moreover, a recent DFT study on Mn(II) porphyrins has enlightened this difficulty: the authors have obtained a (wrong) quartet ground state. It is not until a rather large height $h = 0.37$ Å of the Mn ion with respect to the porphyrin mean plane is reached that the HS state becomes the ground state.[27]

The dependence of spin states ordering with the functional is also recurrent in Fe(II) and Fe(III) porphyrins.[19,20,22,31−33] Even

Received: June 15, 2011
Published: September 12, 2011

dx.doi.org/10.1021/ct2004066 | *J. Chem. Theory Comput.* 2011, 7, 3532–3539

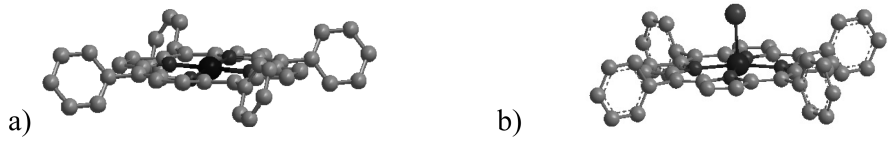

Figure 1. Crystallographic structures of (a) [Mn(II)TPP][26] and (b) [Mn(III)TPPCl].[57] Hydrogen atoms are not depicted, for clarity.

with a hybrid functional such as B3LYP, the spin energetics are not always reliable.[33] More generally, within the last 10 years, a large amount of work in the DFT community has been devoted to the reproduction of spin states ordering within transition metal complexes.[23,28−30,33−40] Some of the main findings that emerged from these studies were (i) the efficiency of the OPTX exchange functional of Handy and Cohen[41] associated with standard local correlation functionals (OPBE, OLYP, etc.) to reproduce low spin energetics of metal complexes,[34,35,39,42] (ii) the design of a modified B3LYP functional, namely B3LYP*, including a weaker exact exchange (ex. ex.) contribution (15%) than the standard one (20%),[28,36] and (iii) the correlation between the HS/LS ordering and the nature of the metal−ligand bonding.[28,29] The latter is of course a direct consequence of the role of the ligand field in the ordering of the lowest electronic states of a metal complex. In the meantime, there have been considerable advances in the design of new families of functionals—the third rung in the so-called Jacob's ladder[43]—especially with the advent of meta-GGAs and hybrid meta-GGAs.[44−46] These functionals have been built with the intent of being as universal as possible, including all chemical elements and a wide range of properties.[44,45]

For all of the above-mentioned reasons, a better analysis of the performance of various functionals for describing Mn(II) and Mn(III) porphyrins became necessary. Such benchmarking may be realized against experimental data or highly accurate *ab initio* calculations as a reference.[23,29,33,47] In this context, explicitly correlated calculations are particularly appealing since (i) they manipulate the exact Hamiltonian and (ii) the multireference character of the wave function gives access to important information with respect to the weights of the different configurations. In a configuration interaction method, the zeroth-order wave function is formed by a linear expansion of Slater determinants. Such a description is accessible by means of Complete Active Space Self-Consistent Field (CASSCF)[48] calculations which incorporate qualitatively the leading electronic configurations distributing n electrons in m molecular orbitals (MOs), defining an active space referenced as CAS[n,m]. At this level of calculation, the so-called static correlation effects are taken into account variationally, provided that the active space is flexible enough. The dynamical correlation effects can be included using second-order perturbation treatment (CASPT2) to produce reference calculations. However, large basis sets and extended active spaces might be necessary to reach convergence in the spectroscopy. Thus, particular attention was paid to (i) the active space characteristics and (ii) the nature of the functional in the low-energy spectroscopy determination.

Several functionals were compared in this study, from GGAs to meta-GGAs, hybrids and hybrid meta-GGAs, including recent and/or already proven efficient functionals, as above-mentioned: (i) GGAs BP86,[49,50] PBE,[51] OPBE,[41] and BLYP;[49,52] (ii) meta-GGAs MO6-L[53] and TPSS;[45] and (iii) hybrid functionals including ex. ex. (value given in parentheses): B3LYP (20%)[54] and B3LYP* (15%),[36] PBE0 (25%),[55] BHandHLYP (50%),[54] and KMLYP (55.7%).[56] The two latter choices were driven by the large exchange energy due to the half-filled d^5 shell in Mn(II). BHandLYP is based on the half-and-half approach of Becke[54] based on 50% Hartree−Fock exchange and 50% BLYP exchange and a correlation functional. Another recent functional, KMLYP, that shows a similar percentage of exact HF exchange (55,7%) has appeared on the basis of the exchange part of Kang and Musgrave.[56] This functional was originally developed to reproduce energy reaction barriers and also contains a built-in reduction of self-interaction errors, which may be too interesting for such issues. Finally, recent meta hybrid functionals have also been investigated, namely, M06 (27%) and M06-2X (54%), from the Minnesota suite[44] completing the local M06-L meta-GGA, and TPSSH (10%) from Staroverov et al.[45] M06 was designed to be efficient for transition metals, while M06-2X was designed for main group elements but incorporates a high content of ex. ex. Finally, TPSS (meta-GGA) and TPSSH[45] were chosen because they are based on a local part, which is the PKZB functional from Perdew et al.,[46] that reproduces the exchange energy to second order in expansion of the density gradient and does not contain self-interaction spurious effects.

Our comparative study based on both the *ab initio* CASPT2 approach and the DFT scheme has been applied on simple Mn(II) and Mn(III) porphyrins, with H atoms in all meso and β positions (named porphin and abbreviated below as P), i.e., $Mn^{II}P$ and $Mn^{III}PCl$. Using the spin-dependent optimized geometries, the adiabatic energy differences for the $Mn^{II}P$ and $Mn^{III}PCl$ systems were calculated. Since some difficulties have been mentioned regarding the spin state ordering of $Mn^{II}P$ with respect to experimental data, the vertical transition from the S = 5/2 was also investigated. The starting geometries were based on X-ray diffraction experimental structures (see Figure 1).

Starting from these structures, we removed the four meso phenyl groups and replaced them with hydrogen atoms leading to the porphin (P) ligand. The use of simple MnP species as a model for more complex architectures has been justified in previous calculations.[16] The resulting structures will be referred to as **a** for the Mn(II) porphyrin and **b** for the Mn(III) porphyrin MnPCl.

Structures **a** and **b** were used as starting geometries to optimize $Mn^{II}P$ and $Mn^{III}PCl$, respectively (see Computational Details). As it was not possible to optimize the structures with CASPT2 methods, we chose to use reference equilibrium geometries resulting from spin-dependent optimizations done with a given GGA (i.e., PBE), with the various possible spin states. The $Mn^{II}P$ optimized structure starting from **a** for sextuplet (S = 5/2) and quartet (S = 3/2) states will be noted as **a-6** and **a-4**, respectively. The $Mn^{III}PCl$ optimized structure from **b** for triplet (S = 1), quintet (S = 2), and septet (S = 3) states will be noted as **b-3**, **b-5**, and **b-7**, respectively.

2. COMPUTATIONAL DETAILS

All of our CASSCF and CASPT2 calculations were performed with the Molcas7.0 package,[58] including atomic natural orbitals (ANO-RCC) as basis sets.[59−61] The one-electron basis sets

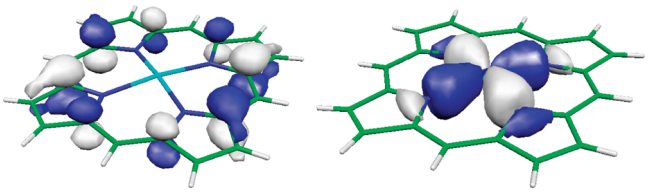

Figure 2. The π-type (left) and σ-type (right) orbitals of the [MnP] complexes from CASSCF calculations.

employed to describe the molecular orbitals (MOs) are derived from primitive ANO-RCC (21s,15p,10d,6f,4 g,2 h), (17s,12p,5d,4f,2 g), (14s,9p,4d,3f,2 g), (14s,9p,4d,3f,2 g), and (8s,4p,3d,1f) for the manganese, chlorine, nitrogen, carbon, and hydrogen atoms, respectively. Following the atomic natural orbital contractions of Widmark, these basis sets were contracted into [7s,6p,5d,3f,2 g,1 h], [4s,3p,1d], [3s,2p,1d], [3s,2p,1d], and [2s1p]. Finally, to avoid the presence of intruder states and to provide a balanced description of open and closed shells, imaginary level and IPEA shifts of 0.20 and 0.25 au (atomic units) were used in the CASPT2 calculations, respectively. All electrons were correlated except those in the core parts. Depending on the number of d electrons, five for the Mn(II) complex and four for the Mn(III), different active spaces can be used for the [MnP] and [MnP]Cl species:

1. CAS[5,5] and CAS[4,5] are the minimal active spaces that consider nothing but the d orbitals and electrons.
2. CAS[14,13] and CAS[13,13] add to the previous one a set of bonding and antibonding porphyrin-localized (π/π^*) orbitals (see Figure 2) within each irreducible representation.
3. CAS[15,14] and CAS[14,14] finally consider a supplementary σ-type orbital (see Figure 2) representing the ion−porphyrin σ bond.Whereas the enlargement from the five-orbital active spaces to the 13-orbital ones is rather natural in light of the extended π system over the porphyrin ring, the inclusion of an additional σ-type orbital deserves some explanation. The importance of ligand-to-metal charge transfers (LMCT), in particular along the σ channel, has been stressed in the ground state from previous DFT-based calculations.[62,63] The 14-orbital active spaces do not discriminate between the σ and π manifolds and allow one to estimate the relative importance of these LMCTs accessible from the wave function expansion.

Dynamical correlation effects were added through the CASPT2[59,64] method that has proven to be an impressive tool used to accurately investigate spectroscopy issues.[65,66] However, extended basis sets combined with rather large active spaces are necessary to reach experimental agreement.[67]

The DFT calculations were performed with the ADF2010 package[68−70] using an all-electron Slater type basis of triple-ζ quality on each atom with polarization functions. Geometry optimizations were made with TZP all-electron basis sets (one polarization function) and single points with TZ2P all-electron basis sets (two polarization functions).[70] All of our calculations were performed using an unrestricted formalism to describe the various spin states. The convergence criteria were fixed to 10^{-6} Hartree for the energy. Several checks were made on calculations (optimizations or single points) carried out with or without symmetry (D_{4h} or C_{2v} for MnP, C_{4v} or C_{2v} for MnPCl), showing that symmetry contraints do not greatly affect the results. For instance, optimizations lead to distance differences less than 0.02 Å and energy differences less than 0.04 eV.

3. MN(II) PORPHYRINS

Geometry optimizations for the sextet and quadruplet states performed with the PBE functional gave flat porphyrin systems, as already pointed out in the literature.[20,27] Indeed, it is known that the porphyrin ring is rather flexible, precluding a reliable investigation of minima on the potential energy surface.[71,72] The Mn−N distance for **a-6** species was 2.07 Å (exp. 2.085 Å[26]) and 2.00 Å for **a-4**. Optimizations with BLYP, OBPE, B3LYP, and M06 gave very similar geometries with distances ranging from 2.07 to 2.085 Å for **a-6** and 2.00 to 2.02 Å for **a-4**. The decrease of Mn−N distances between the $S = 5/2$ and the $S = 3/2$ structures is in line with the depopulation of the mainly $d_{x^2-y^2}$ antibonding orbital.

In order to check their consistency and convergence, the CASPT2 results were calibrated using several active spaces on the experimental structure **a** (see Table 1). In agreement with experimental observations, the three active spaces CAS[5,5], CAS[14,13], and CAS[15,14] give rise to a sextet ($S = 5/2$) ground state. As seen in Table 1, the spin gap between the $S = 5/2$ (HS) and $S = 3/2$ (IS) states is almost not affected by the active space enlargement. The comparison between CAS[14,13] and CAS[15,14] is however instructive. Indeed, the inclusion of the σ-type orbital does not lead to any significant modification of the wave functions' structures. It should be stressed that for both spin-states, the main configuration holds a similar weight.

Both vertical and adiabatic energy differences (see Figure 3) were computed. $\Delta E_{\mathbf{a}}^{\mathrm{vert}}$ uses the high-spin state geometry **a-6**, whereas $\Delta E_{\mathbf{4-6}}^{\mathrm{adia}}$ relies on the quartet and sextet optimized geometries **a-4** and **a-6**.

Table 2 gathers the results obtained with the various functionals defined above, compared to the reference CAS[15,14]PT2 values for both types of transition energy.

The first check was to correctly reproduce the experimentally known ordering, i.e., the sextet being the ground state thus corresponding to a positive energy gap. Clearly, GGAs and meta-GGAs are unable to reproduce this ordering, yielding a negative gap. It should be mentioned nevertheless that using the OPTX exchange potential (OLYP and OPBE) results in a weak spin gap, which becomes even positive with OLYP for the vertical transition. The most satisfactory behavior is obtained when including ex. ex., in hybrids or hybrid meta-GGAs functionals. But even in that case, the expected ordering is not obtained in all cases as B3LYP* (15%), B3LYP (20%), and PBE0 (25%) give again a wrong ordering of the gaps for the vertical transition.

At this stage, the PBE optimized geometries might be questionable. Therefore, the geometries and corresponding adiabatic energy differences were calculated for a selection of functionals (see Table 3).

It is remarkable that OPBE and B3LYP give now qualitatively good ordering, with a sextet ground state, while BLYP and BPE still fail in reproducing the expected ordering.

From a qualitative point of view, there are clearly three major behaviors: GGAs and meta-GGAs, which are far from experimental agreement (except the OPTX-based ones), OPTX derived (OPBE and OLYP) and hybrid functionals with a low percentage of ex. ex. for which the result is ambiguous and depends on the molecular structure, and finally the hybrids with

Table 1. CASPT2 Quartet−Sextet Vertical Spin Gap (eV) for the Experimentally Derived Structure a, Using Different Active Spaces

active space	gap (eV)	weight of the main configuration for $S = 5/2$	weight of the main configuration for $S = 3/2$
CAS[5,5]	1.40	1.00	0.98
CAS[14,13]	1.36	0.85	0.83
CAS[15,14]	1.37	0.84	0.83

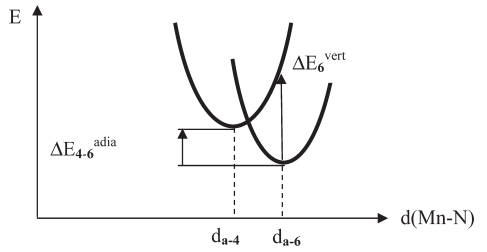

Figure 3. Potential energy curves for sextet and quadruplet spin states vs. d(Mn−N) distance in the porphyrin and definitions of the spin gaps as estimated in the CASPT2 and DFT evaluations.

at least 50% ex. ex. and hybrid meta-GGAs which always lead to the expected sextet ground state.

We turn now to a more quantitative comparison, based on the CAS[15,14]PT2 values. Hybrids with less than 25% ex. ex., even if they give the expected sign for the vertical gap, do not perform well for numerical values. The best agreement—qualitatively and quantitatively—is obtained for hybrid functionals with a higher HF percentage, i.e., BHandHLYP and KMLYP, being the only ones to reproduce the good ordering in the vertical transition, although the numerical agreement is less favorable. Among the hybrid meta-GGAs, TPSSH gives a too low gap while M06 and M06-2X give a rather good agreement with the CAS[15,14]PT2 calculation.

We should mention that we checked that the electronic configurations of both sextet and quadruplet states obtained with both DFT and CAS approaches (the latter showing only one major configuration as above-mentioned) were the same. For the high spin state, the expected $(d_{z^2})^1(d_{xy})^1(d_{xz},d_{yz})^2(d_{x^2-y^2})^1$ configuration was obtained. The lowest quartet state was also found to be $(d_{z^2})^1(d_{xy})^1(d_{xz},d_{yz})^3(d_{x^2-y^2})^0$, in agreement with the CAS[15,14] leading configuration. The spin contaminations that may reveal some mixing with higher states were checked for both spin states. It was found to be very low, as could be expected for the high spin state (S^2 = 8.75 to 8.77 for an expected one of 8.75). For the quartet state with an expected value of S^2 = 3.75, we obtained, most of the time, weak spin contamination with S^2 between 3.77 and 4 (i.e., < 10%) for GGAs, meta-GGAs, and hybrids, while three local functionals (M06-L, OPBE, and OLYP) gave a slightly larger value close to 4.2.

We should also mention that due to the differences obtained in the various B3LYP gaps (almost 0 eV for PBE optimized geometries and 0.58 eV for B3LYP optimized geometries), we also checked the consistency of the electronic configuration by calculating the gap on one geometry (B3LYP or PBE ones) restarting with the electron density obtained from the other

Table 2. Spin Gaps ΔE_6^{vert} and $\Delta E_{4\text{-}6}^{adia}$ in eV Calculated by DFT Methods and CAS[15,14]PT2[a]

	ΔE_6^{vert}	$\Delta E_{4\text{-}6}^{adia}$
	GGA	
PBE	−0.28	−0.49
OPBE	−0.16	−0.14
BLYP	−0.4	−0.59
OLYP	0.04	−0.19
BP86	−0.28	−0.55
	hybrid	
B3LYP*	0.06	−0.2
B3LYP	0.23	−0.03
PBE0	0.5	−0.01
BHandHLYP	1.07	0.92
KMLYP	0.99	1.03
	meta-GGA	
M06-L	−0.18	−0.62
TPSS	−0.43	−0.76
	meta-hybrid	
M06	0.71	0.83
M06-2X	1.49	1.18
TPSSH	0.32	0.16
CASPT2	1.03	0.49

[a] All stuctures were optimized using the PBE functional.

Table 3. Adiabatic Energy Gap between the Quadruplet and Sextet States, with Geometries Optimized for Each Functional

functional	$\Delta E_{4\text{-}6}^{adia}$
PBE	−0.39
OPBE	0.06
BLYP	−0.43
B3LYP	0.58
M06	0.30

geometry (respectively PBE or B3LYP ones). This was accompanied by a check of the electron configurations, especially in the quartet states. The results were very similar to the ones above-mentioned (obtained without restarting densities), with a gap of 0.07 eV for the PBE geometries using the restart from B3LYP geometries and a gap of 0.55 eV for the B3LYP geometries using the restart from PBE geometries. The electronic structures were also checked to be consistent with the sextet and quartet state configurations described above.

As another check, we also explored the comparison of the potential energy curves as a function of the Mn height above the porphyrin plane, calculated for the [Mn^{II}P] complex from experimentally derived structure **a**. This key parameter was chosen due to ambiguous determinations through previous X-ray and theoretical studies.[26,27,73] As depicted in Figure 4, whatever the position of the manganese ion, the vertical quartet−sextet gap is at least 1.37 eV. Let us stress that the S = 5/2 potential energy curve is rather flat, the energy variation being less than 0.1 eV for $h \leq 0.45$ Å. This result might support the reported difficulties in [MnP] structure determinations since the

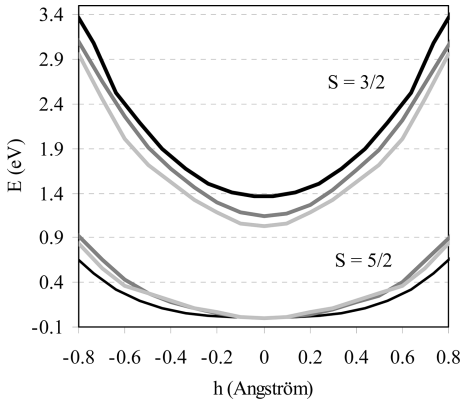

Figure 4. Potential energy curves with respect to the Mn ion displacement *h* for the [MnP] complex **a** for $S = 5/2$ and $S = 3/2$ states. Black: CASPT2. Dark gray: DFT/KMLYP. Light gray: DFT/M06. Zero energy reference taken as the $h = 0$ point for $S = 5/2$ state.

Mn(II) ion has the ability to be displaced out of the plane under weak external perturbations.[25,26]

At this stage, the KMLYP functional which displays the best overall agreement also gives a potential energy curve quite close to the CASPT2 result. M06 also closely reproduces the results from KMLYP, but with a smaller quartet−sextet gap, as was already observed in Table 2. Yet it gives a very satisfactory reproduction of the ground state curve.

From our comparison and previously reported ones, it is clear that the correct reproduction of the ground state of $Mn^{II}P$ species remains challenging for quantum chemical modeling. The inclusion of HF exchange helps to recover the high spin ground state, in line with the classical observation that high spin states are favored by including some exact exchange in the functional.[28,29]

4. MN(III) PORPHYRINS

The spin energetics of the [MnPCl] species were investigated using again optimized structures starting from the experimental structure **b**, for each of the three spin states: triplet, quintet, and septet. The latter state is very often encountered in the Mn^{III} porphyrin physicochemistry and corresponds to a formally Mn^{II} ($S = 5/2$) ion ferromagnetically coupled to a $S = 1/2$ radical on the porphyrin. The agreement between the structural parameters optimized for the quintet ground state with experimental data was very satisfactory, with a mean Mn−N distance of 2.04 Å (exp. 2. 015 Å), d(Mn−Cl) = 2.30 Å (exp. 2.30 Å), and a Mn out of plane displacement of 0.30 Å (exp. 0.32 Å).

The geometry optimization for the $S = 3$ state yields longer Mn−N distances (2.098 Å). Accordingly, the Kohn−Sham orbitals clearly show that the $d_{x^2-y^2}$ is occupied—as expected for a high spin Mn(II) ion—and the spin densities give 4.5 on the Mn ion and a total of 1.06 delocalized on the four *meso* carbon atoms. This electronic structure supports the $[Mn^{II}P^{\bullet}]$ nature of the septet $[Mn^{III}P]^{+}$ state in MnPCl.

In a first step, we explored the active space for CASPT2 calculations, starting from the experimentally derived structure **b**. The results are shown in Table 4. As for Mn(II) complexes, a first minimal active space (CAS[4,5]) has been used and leads to an $S = 2$ ground state ($^5A_2$) followed by two low-lying triplets $^3B_2$ and $^3B_1$ at 1.65 and 2.11 eV, respectively. Then, by enlarging the active space to CAS[12,13], a charge transfer state $[Mn(II)P^{\bullet}]^{+}$ ($^7A_2$) can be described. It arises from the promotion of a π electron of the porphyrin ring into the vacant $d_{x^2-y^2}$ orbital of Mn as already mentioned above in the DFT study. This state appears to be the first excited state at the CAS[12,13]PT2 level. In order to properly account for any charge redistributions between the Mn ion and the porphyrin ring, the 14-orbital active space has been tested, including both σ and π channels. $^5A_2$ remains the ground state. $^7A_2$ is shifted to much higher energies, i.e., 1.74 eV above $^5A_2$, while the triplets are stabilized with respect to the previous calculation. Thus, it is clear from this monitoring that the correct description of the σ transfer is crucial in the ordering of spin-states of Mn(III) complexes. Any successive enlargement of the active space led to no visible modification of the spectroscopy.

We have then used the CAS[14,14]PT2 results as reference to compare all DFT results obtained for each optimized geometry in each spin state. The results are summarized in Table 5.

The first conclusion is that whatever the functional, the expected quintet ground state is obtained. This is in contrast with the various differences observed with the $Mn^{II}P$ species. Apart from this first qualitative observation, the concern remains

Table 4. CASPT2 Low-Energy Vertical Spectroscopy (eV) of the [MnPCl] Complex Calculated with Different Active Spaces from Structure b[a]

active space	$^3A_2$	$^3B_2$	$^7A_2$
CAS[4,5]	2.11	1.65	
CAS[12,13]	2.05	1.61	1.41
CAS[14,14]	1.44	1.53	1.74

[a] The reference energy is the quintet state $^5A_2$ (C_{2v}).

Table 5. Adiabatic Energy Gaps (eV) of the Lowest Triplet ($S = 1$) and Septet ($S = 3$) States, Respectivley[a]

	ΔE_{3-5}^{adia}	ΔE_{7-5}^{adia}
	GGA	
PBE	0.42	1.55
OPBE	0.83	1.32
BLYP	0.37	1.50
OLYP	0.78	1.29
BP86	0.42	1.52
	hybrid	
B3LYP*	0.7	1.39
B3LYP	0.45	1.47
PBE0	1.14	1.67
BHandHLYP	1.21	1.07
KMLYP	1.28	1.11
	meta-GGA	
M06-L	1.27	1.82
TPSS	0.37	1.80
	meta-hybrid	
M06	1.45	1.54
M06-2X	1.83	1.15
TPSSH	0.55	1.72
CAS[14,14]PT2	1.51	1.10

[a] $\Delta E_{3\text{-}5}^{adia}$ and $\Delta E_{7\text{-}5}^{adia}$, with reference to the quintet ground state.

about the ordering of excited spin states. In these relaxed geometries, the $S = 3$ spin state at the CAS[14,14]PT2 level is found to be lower than the $S = 1$ state, whereas GGAs, meta-GGAs, and some hybrids yield the opposite result. The two hybrids KMLYP and BHandHLYP give a very satisfactory quantitative agreement, which again can be related to the stabilization of high spin states due to a high ex. ex. content within these functionals. The results of the M06 and M06-2X meta-hybrid functionals are also in rather good agreement with the CASPT2 orderings.

The spin contamination has been checked for the three states ($S^2 = 6$ for the ground state, $S^2 = 2$ for the triplet, and $S^2 = 12$ for the septet state). Almost no deviation is observed for the quintet state with all S^2 values in the range 6.03−6.09, while deviations are below 10% for the triplet state (almost all being between 2.02 and 2.07). Finally, for the septet state, again very low deviations are obtained with all values between 12.04 and 12.16.

As for Mn(II) species, we have analyzed the Kohn−Sham orbitals of the lowest triplet state that was obtained in DFT and compared it to the major configuration given by the CAS approach. For the high spin state, the expected $(d_{xz}d_{yz})^2(d_{xy})^1(d_{z^2})^1(d_{x^2-y^2})^0$ configuration was obtained, resulting in a $^3A_2$ symmetry in the C_{2v} point group as obtained in the CASPT2 C_{2v} calculations. The lowest triplet state yielded the same configuration: $(d_{xz}d_{yz})^2(d_{xy})^2(d_{z^2})^0(d_{x^2-y^2})^0$ as the main one found in the CASPT2 calculation and corresponding to the $^3A_2$ state in C_{2v} symmetry.

At this stage, we would like to comment on the choice of CASPT2 calculations as a reference in this particular case. Indeed, to obtain a balanced description of open and closed shells along the perturbative treatment, one has to include a so-called IPEA (ionization potential−electronic affinity) shift in the zeroth-order Hamiltonian.[74] The default value of 0.25 au as set by default in the current Molcas package usually gives excellent results. Nevertheless, this choice has been questioned on two occasions: (i) the case of magnetically coupled metals where it was found that the originally proposed zeroth-order Hamiltonian (corresponding to an IPEA set to 0.00 au) led to better description of the magnetic coupling[75]and (ii) in the evaluation of the adiabatic gap (between $S = 0$ and $S = 2$ spin states) for Fe(II) spin-crossover systems where it is suggested that a proper description of the gap requires an IPEA shift no less than 0.50 au.[76] For the former, the spectroscopy is characterized by states with identical numbers of open shells. In contrast, such number changes along the $S = 0$ to $S = 2$ transition. In a first step, we checked the impact of the IPEA shift on the low-energy spectroscopy of the Mn(II) species. The change in the quartet−sextet adiabatic gap appears to be less than 0.20 eV when going from the default value 0.25 au to the very high 0.75 au. In particular, no change is observed in the ordering of spin states. Thus, the standard 0.25 au value is suitable for calculations upon Mn(II) species, keeping in mind an error bar of ±0.10 eV. On the other hand, the low-energy spectrum of Mn(III) species has to be treated more carefully. Even for a large IPEA shift value up to 1.00 au, the quintet state remains the ground state. However, the septet−quintet gap appears to be more sensitive to this parameter. Let us stress that the number of open shells reaches six for the heptet state, which involves an intramolecular electron transfer. As previously reported in the literature, the description of such a phenomenon requires larger values of the IPEA shift (∼0.5 au). Considering the CASPT2 limitations, one may conclude at this stage that the excited triplet and septet states are expected to lie relatively close in energy.

5. DISCUSSION

The present study has been intended to check the behavior of various types of functionals to reproduce qualitatively and—when possible—quantitatively the energetic ordering of the lowest spin states in Mn(II) and Mn(III) porphyrins. Our conclusion is that in Mn(III) species, all types of functionals are able to reproduce at least qualitatively and—for some—quantitatively the spin states ordering. However, the story is completely different for Mn(II) porphyrins, and we will focus the discussion on these systems.

In the following, we will first position our own results in the light of recent literature in spin states DFT benchmarking. Then, we will give some comments based first on the chemical nature of Mn(II), then on the choice of functionals that seems to result from this particular nature.

Our conclusion about the good efficiency of high exchange hybrid functionals is not completely in line with previous studies performed on the functionals to reproduce spin states ordering in 3d transition metal complexes. Indeed, most analogous comparative studies have been conducted on Fe^{II} and Fe^{III} complexes[23,28,30,32,39,42,77−80] because they are ubiquitous in active sites of metalloenzymes, within mononuclear or polynuclear clusters with magnetic coupling, and because this transition metal is very much used in spin-crossover materials. As mentioned in the Introduction, some constant conclusions emerged from these numerous studies, about the very efficient behavior of the exchange potential OPTX and about the good behavior of B3LYP* with a decrease of ex. ex. compared to the standard B3LYP functional. Yet the efficiency of B3LYP* for spin state orderings proved not to be universal.[32,42,80,81] Finally, all of these observations were nicely rationalized by some authors, on the basis of the nature of the ligand bonding.[29,32,39] High spin complexes are favored with ligands giving rise to more ionic bonding such as O or N donor ligands, whereas S, P, or C donor ligands are bonded with more covalent character, thus favoring a higher ligand field and lower spin ground states. Thus, hybrid functionals with a higher ex. ex. percentages are expected to perform better within ionic complexes with low covalence, whereas with complexes involving a more covalent bonding, hybrid functionals with a low percentage of ex. ex. are expected to be better.[32,39,47]

Thus, this rationalization in terms of chemical features can be extended to our case. Indeed, Mn(II) is very special among the 3d transition series. It is well-known by coordination chemists that this ion gives almost exclusively high spin ground state complexes[82] except with very strong field ligands such as CO, cyanide, or alkyle/aryle ligands. The manganese(II) ion in most of the ligand environments is known to behave as a noninteracting large sphere. The metallocene family is a typical example of this unique character, as all 3d metallocenes exhibit a low spin ground state except Mn(II). The manganocene complex ($Mn^{II}Cp_2$, $Cp = C_5H_5$) has been much studied using EPR and NMR solid state spectroscopies.[83,84] At very low temperatures, it exhibits antiferromagnetic coupling of $S = 5/2$ units, due to a solid-state structure where the Cp ligands bridge two Mn(II) ions.[84] Moreover, NMR paramagnetic studies also revealed that manganocene was unique among other metallocenes because the metal−Cp ring bond was much less covalent than that of

nickelocene and cobaltocene.[84] Another remarkable feature is that when substituting the Cp rings with alkyle groups, the derived manganocene exhibited a low spin ground state.[84] This particular example illustrates several features of Mn(II) chemistry: (i) Mn(II) gives preferentially low covalent complexes and a high spin ground state even with the Cp ligand, known to favor low spin complexes, and it is necessary to substitute this ligand with alkyl groups in order to get a low spin ground state. (ii) The low covalence is correlated to the high spin ground state. (iii) DFT benchmarking on this particular case has yielded ambiguous results.[28,29]

The particular stability of the half filled d shell in Mn(II) due to a high exchange contribution is a key point. But Fe^{III}—also a d^5 ion—does not behave the same. Yet, the latter is more positively charged, allowing ligands to get closer, thus favoring strong field environments, thus lower spin states. In fact, Fe(III) complexes exhibit various types of spin states, depending on their coordination environment.

All of these considerations give support to our results for $Mn^{II}P$ species, pointing to the need of increasing the ex. ex. contribution in hybrid functionals in order to properly describe the nature of Mn(II) complexes, unless particularly covalent bonds are expected. Indeed, the proper description of the exchange term and its correct balance with the correlation part is clearly very critical for Mn(II) species. In this context, the OPTX exchange constructed by fitting the HF exchange on atoms[41] behaves remarkably well and is the only GGA able to compete with hybrid functionals. But in order to get a quantitative agreement, inclusion of a high content of ex. ex. is desirable, and the tuning of the percentage has a direct effect on the efficiency of the hybrid, as already above-mentioned.

6. CONCLUSION

The present study was devoted to the evaluation of the low-energy spectroscopy of Mn-porphyrins through *ab initio* methods and to the comparison with DFT methods. For both Mn(II) and Mn(III) species, CASPT2 calculations were first conducted with different active spaces. In the case of Mn(II) compounds, the experimental spin ordering is recovered even with a minimal active space. However, the spectroscopy of Mn(III) complexes requires a larger active space to reach a correct description of the low-energy spectrum, featuring a capital part played by both σ- and π-type orbitals. This is reminiscent of the experimentally very different spectroscopies of Mn(II)P and Mn(III)P, well documented in the literature (see for instance ref 1).

These studies have allowed us to design a reliable DFT approach of Mn-porphyrin complexes. Indeed, as already mentioned in many instances, we fuel some other arguments—if necessary—that the choice of a functional is particularly crucial in transition metal complexes, where the spin state ordering may be complicated due to subtle interplay between d shell effects and the metal−ligand bonding nature. As in previously published studies, GGAs and meta-GGAs fail to reproduce the correct ordering in the Mn(II) sextet−quartet states as well as some hybrids, whereas the correct one is recovered with hybrids with a high content of ex. ex. such as KMLYP, BHANDHLYP, or to a lesser extent M06.

We must emphasize again the very special nature of the Mn(II) ion among other 3d metal ions, being a very large ion with a half filled d shell, that is known by coordination chemists to give mainly high spin species (except with very strong field ligands).[82] We believe that this case is another "niche" where we cannot simply apply standard DFT methods. We must think of the chemistry behind the system in order to adapt the method and make an extensive usage of the experiences in the various theoretical approaches already published. The present study is another illustration of what has already been pointed out in some reflections published in recent years, about the pursuit of the "divine" functional.[43,78,85,86]

AUTHOR INFORMATION

Corresponding Author

*E-mail: vincent.robert@ens-lyon.fr, vrobert@unistra.fr (V.R.); pascale.maldivi@cea.fr (P.M.).

Present Addresses

[||]LITEN/DEHT/LPCEM, CEA-Grenoble, 17 rue des Martyrs, 38054 Grenoble cedex 9, France

ACKNOWLEDGMENT

A.C. wishes to thank research funding from the European Community under the FP6 - Marie Curie Host Fellowships for Early Stage Research Training (EST) "CHEMTRONICS" Contract Number MEST-CT-2005-020513".

REFERENCES

(1) Boucher, L. J. *Coord. Chem. Rev.* **1972**, *7*, 289–329.
(2) Scheidt, W. R. *Acc. Chem. Res.* **1977**, *10*, 339–345.
(3) Zerner, M.; Gouterma, M. *Theor. Chim. Acta* **1966**, *4*, 44.
(4) Gunter, M. J.; Turner, P. *Coord. Chem. Rev.* **1991**, *108*, 115–161.
(5) La Mar, G. N.; Walker, F. A. *The Porphyrins*; Academic Press: New York, 1979; Vol. 4.
(6) Wang, C. Q.; Shalyaev, K. V.; Bonchio, M.; Carofiglio, T.; Groves, J. T. *Inorg. Chem.* **2006**, *45*, 4769–4782.
(7) Collman, J. P.; Zhang, X. M.; Lee, V. J.; Uffelman, E. S.; Brauman, J. I. *Science* **1993**, *261*, 1404–1411.
(8) Groves, J. T. *Proc. Natl. Acad. Sci. U.S.A.* **2003**, *100*, 3569–3574.
(9) Beletskaya, I.; Tyurin, V. S.; Tsivadze, A. Y.; Guilard, R.; Stern, C. *Chem. Rev.* **2009**, *109*, 1659–1713.
(10) Kulikov, O. V.; Schmidt, I.; Muresan, A. Z.; Lee, M. A. P.; Bocian, D. F.; Lindsey, J. S. *J. Porph. Phtalo.* **2007**, *11*, 699–712.
(11) Li, C.; Fan, W. D.; Lei, B.; Zhang, D. H.; Han, S.; Tang, T.; Liu, X. L.; Liu, Z. Q.; Asano, S.; Meyyappan, M.; Han, J.; Zhou, C. W. *App. Phys. Lett.* **2004**, *84*, 1949–1951.
(12) Li, Q. L.; Mathur, G.; Gowda, S.; Surthi, S.; Zhao, Q.; Yu, L. H.; Lindsey, J. S.; Bocian, D. F.; Misra, V. *Adv. Mater.* **2004**, *16*, 133–137.
(13) Duclairoir, F.; Dubois, L.; Calborean, A.; Fateeva, A.; Fleury, B.; Kalaiselvan, A.; Marchon, J. C.; Maldivi, P.; Billon, M.; Bidan, G.; de Salvo, B.; Delapierre, G.; Buckley, J.; Huang, K.; Barattin, R.; Pro, T. *Int. J. Nanotechnol.* **2010**, *7*, 719–737.
(14) Daku, L. M. L.; Castaings, A.; Marchon, J. C. *Inorg. Chem.* **2009**, *48*, 5164–5176.
(15) Liao, M. S.; Scheiner, S. *J. Comput. Chem.* **2002**, *23*, 1391–1403.
(16) Liao, M. S.; Scheiner, S. *J. Chem. Phys.* **2002**, *117*, 205–219.
(17) Ghosh, A.; Vangberg, T.; Gonzalez, E.; Taylor, P. *J. Porph. Phtalo.* **2001**, *5*, 345–356.
(18) Liu, C. G.; Guan, W.; Song, P.; Yan, L. K.; Su, Z. M. *Inorg. Chem.* **2009**, *48*, 6548–6554.
(19) Scherlis, D. A.; Estrin, D. A. *Int. J. Quantum Chem.* **2002**, *87*, 158–166.
(20) Leung, K.; Rempe, S. B.; Schultz, P. A.; Sproviero, E. M.; Batista, V. S.; Chandross, M. E.; Medforth, C. J. *J. Am. Chem. Soc.* **2006**, *128*, 3659–3668.

(21) Baerends, E. J.; Ricciardi, G.; Rosa, A.; van Gisbergen, S. J. A. *Coord. Chem. Rev.* **2002**, *230*, 5–27.
(22) Liao, M. S.; Watts, J. D.; Huang, M. J. *J. Comput. Chem.* **2006**, *27*, 1577–1592.
(23) Vancoillie, S.; Zhao, H. L.; Radon, M.; Pierloot, K. *J. Chem. Theory Comput.* **2010**, *6*, 576–582.
(24) Gonzalez, B.; Kouba, J.; Yee, S.; Reed, C. A. *J. Am. Chem. Soc.* **1975**, *97*, 3247–3249.
(25) Kirner, J. F.; Reed, C. A.; Scheidt, W. R. *J. Am. Chem. Soc.* **1975**, *97*, 2557–2563.
(26) Kirner, J. F.; Reed, C. A.; Scheidt, W. R. *J. Am. Chem. Soc.* **1977**, *99*, 1093–1101.
(27) Liao, M. S.; Watts, J. D.; Huang, M. J. *Inorg. Chem.* **2005**, *44*, 1941–1949.
(28) Salomon, O.; Reiher, M.; Hess, B. A. *J. Chem. Phys.* **2002**, *117*, 4729–4737.
(29) Swart, M. *Inorg. Chim. Acta* **2007**, *360*, 179–189.
(30) Swart, M.; Groenhof, A. R.; Ehlers, A. W.; Lammertsma, K. *J. Phys. Chem. A* **2004**, *108*, 5479–5483.
(31) Liao, M. S.; Watts, J. D.; Huang, M. J. *J. Phys. Chem. A* **2007**, *111*, 5927–5935.
(32) Pierloot, K.; Vancoillie, S. *J. Chem. Phys.* **2008**, *128*, 34104.
(33) Ghosh, A.; Persson, B. J.; Taylor, P. R. *J. Biol. Inorg. Chem.* **2003**, *8*, 507–511.
(34) Conradie, J.; Ghosh, A. *J. Chem. Theory Comput.* **2007**, *3*, 689–702.
(35) Noodleman, L.; Han, W. G. *J. Biol. Inorg. Chem.* **2006**, *11*, 674–694.
(36) Reiher, M.; Salomon, O.; Hess, B. A. *Theor. Chem. Acc.* **2001**, *107*, 48–55.
(37) Shaik, S.; Chen, H.; Janardanan, D. *Nature Chem.* **2011**, *3*, 19–27.
(38) Sorkin, A.; Iron, M. A.; Truhlar, D. G. *J. Chem. Theory Comput.* **2008**, *4*, 307–315.
(39) Swart, M. *J. Chem. Theory Comput.* **2008**, *4*, 2057–2066.
(40) Schultz, N. E.; Zhao, Y.; Truhlar, D. G. *J. Phys. Chem. A* **2005**, *109*, 4388–4403.
(41) Handy, N. C.; Cohen, A. J. *Mol. Phys.* **2001**, *99*, 403–412.
(42) Fouqueau, A.; Casida, M. E.; Lawson Daku, L. M.; Hauser, A.; Neese, F. *J. Chem. Phys.* **2005**, *122*, 44110.
(43) Perdew, J. P.; Ruzsinszky, A.; Constantin, L. A.; Sun, J. W.; Csonka, G. I. *J. Chem. Theory Comput.* **2009**, *5*, 902–908.
(44) Zhao, Y.; Truhlar, D. G. *Theor. Chem. Acc.* **2008**, *120*, 215–241.
(45) Staroverov, V. N.; Scuseria, G. E.; Tao, J. M.; Perdew, J. P. *J. Chem. Phys.* **2003**, *119*, 12129–12137.
(46) Perdew, J. P.; Kurth, S.; Zupan, A.; Blaha, P. *Phys. Rev. Lett.* **1999**, *82*, 2544–2547.
(47) Ganzenmuller, G.; Berkaine, N.; Fouqueau, A.; Casida, M. E.; Reiher, M. *J. Chem. Phys.* **2005**, 122.
(48) Roos, B. O.; Taylor, P. R. *Chem. Phys.* **1980**, *48*, 157–173.
(49) Becke, A. D. *Phys. Rev. A* **1988**, *38*, 3098–3100.
(50) Perdew, J. P. *Phys. Rev. B* **1986**, *33*, 8822–8824.
(51) Perdew, J. P.; Burke, K.; Ernzerhof, M. *Phys. Rev. Lett.* **1996**, *77*, 3865–3868.
(52) Lee, C. T.; Yang, W. T.; Parr, R. G. *Phys. Rev. B* **1988**, *37*, 785–789.
(53) Zhao, Y.; Truhlar, D. G. *J. Chem. Phys.* **2006**, *125*, 18.
(54) Becke, A. D. *J. Chem. Phys.* **1993**, *98*, 1372–1377.
(55) Perdew, J. P.; Burke, K.; Ernzerhof, M. *J. Chem. Phys.* **1996**, *105*, 9982.
(56) Kang, J. K.; Musgrave, C. B. *J. Chem. Phys.* **2001**, *115*, 11040.
(57) Cheng, B. S.; Fries, P. H.; Marchon, J. C.; Scheidt, W. R. *Inorg. Chem.* **1996**, *35*, 1024–1032.
(58) Karlstrom, G.; Lindh, R.; Malmqvist, P. A.; Roos, B. O.; Ryde, U.; Veryazov, V.; Widmark, P. O.; Cossi, M.; Schimmelpfennig, B.; Neogrady, P.; Seijo, L. *Comput. Mater. Sci.* **2003**, *28*, 222–239.
(59) Andersson, K.; Malmqvist, P. A.; Roos, B. O. *J. Chem. Phys.* **1992**, *96*, 1218–1226.
(60) Roos, B. O.; Lindh, R.; Malmqvist, P. A.; Veryazov, V.; Widmark, P. O. *J. Phys. Chem. A* **2004**, *108*, 2851–2858.
(61) Roos, B. O.; Lindh, R.; Malmqvist, P. A.; Veryazov, V.; Widmark, P. O. *J. Phys. Chem. A* **2005**, *109*, 6575–6579.
(62) Cheng, R. J.; Lee, C. H.; Chao, C. W. *Chem. Commun.* **2009**, 2526–2528.
(63) Cheng, R. J.; Wang, Y. K.; Chen, P. Y.; Han, Y. P.; Chang, C. C. *Chem. Commun.* **2005**, 1312–1314.
(64) Andersson, K.; Malmqvist, P. A.; Roos, B. O.; Sadlej, A. J.; Wolinski, K. *J. Phys. Chem.* **1990**, *94*, 5483–5488.
(65) Sadoc, A.; Broer, R.; De Graaf, C. *J. Chem. Phys.* **2007**, *126*, 134709.
(66) Sadoc, A.; De Graff, C.; Broer, R. *Phys. Rev. B* **2007**, *75*, 165116.
(67) Kepenekian, M.; Robert, V.; Le Guennic, B.; De Graaf, C. *J. Comput. Chem.* **2009**, *30*, 2327–2333.
(68) *SCM*; Theoretical Chemistry, Vrije Universiteit: Amsterdam, The Netherlands, 2010.
(69) Fonseca Guerra, C.; Snijders, J. G.; te Velde, G.; Baerends, E. J. *Theor. Chem. Acc.* **1998**, *99*, 391–403.
(70) te Velde, G.; Bickelhaupt, F. M.; Baerends, E. J.; Fonseca Guerra, C.; Van Gisbergen, S. J. A.; Snijders, J. G.; Ziegler, T. *J. Comput. Chem.* **2001**, *22*, 931–967.
(71) Vangberg, T.; Ghosh, A. *J. Am. Chem. Soc.* **1999**, *121*, 12154–12160.
(72) Paulat, F.; Praneeth, V. K. K.; Nather, C.; Lehnert, N. *Inorg. Chem.* **2006**, *45*, 2835–2856.
(73) Kirner, J. F.; Scheidt, W. R. *Inorg. Chem.* **1975**, *14*, 2081–2086.
(74) Ghigo, G.; Roos, B. O.; Malmqvist, P. A. *Chem. Pys. Lett.* **2004**, *396*, 142–149.
(75) Queralt, N.; Taratiel, D.; de Graaf, C.; Caballol, R.; Cimiraglia, R.; Angeli, C. *J. Comput. Chem.* **2008**, *29*, 994–1003.
(76) Kepenekian, M.; Robert, V.; Le Guennic, B. *J. Chem. Phys.* **2009**, 131.
(77) Deeth, R. J.; Fey, N. *J. Comput. Chem.* **2004**, *25*, 1840–1848.
(78) Ghosh, A. *J. Biol. Inorg. Chem.* **2006**, *11*, 712–724.
(79) Conradie, J.; Ghosh, A. *J. Phys. Chem. B* **2007**, *111*, 12621–12624.
(80) Fouqueau, A.; Mer, S.; Casida, M. E.; Daku, L. M. L.; Hauser, A.; Mineva, T.; Neese, F. *J. Chem. Phys.* **2004**, *120*, 9473–9486.
(81) Zein, S.; Borshch, S. A.; Fleurat-Lessard, P.; Casida, M. E.; Chermette, H. *J. Chem. Phys.* **2007**, *126*, 14105.
(82) *Advanced Inorganic Chemistry*, 6th ed.; Cotton, F. A., Wilkinson, G., Eds.; Wiley - Interscience: New York, 1999.
(83) Hebendanz, N.; Kohler, F. H.; Muller, G.; Riede, J. *J. Am. Chem. Soc.* **1986**, *108*, 3281–3289.
(84) Heise, H.; Kohler, F. H.; Xie, X. L. *J. Magn. Reson.* **2001**, *150*, 198–206.
(85) Ghosh, A. *J. Biol. Inorg. Chem.* **2006**, *11*, 671–673.
(86) Mattson, A. E. *Science* **2002**, *298*, 759–760.